Science Advances
AAAS

advances.sciencemag.org/cgi/content/full/4/7/eaar2904/DC1

Supplementary Materials for

Molecularly selective nanoporous membrane-based wearable organic electrochemical device for noninvasive cortisol sensing

Onur Parlak*, Scott Tom Keene, Andrew Marais, Vincenzo F. Curto, Alberto Salleo*

*Corresponding author. Email: parlak@stanford.edu (O.P.); asalleo@stanford.edu (A.S.)

Published 20 July 2018, *Sci. Adv.* **4**, eaar2904 (2018)
DOI: 10.1126/sciadv.aar2904

This PDF file includes:

Supplementary Materials

All chemicals and solvents were of reagent grade and were used without further purification unless otherwise stated. Potassium dihydrogen phosphate (KH_2PO_4, ≥99.0%), dipotassium hydrogen phosphate (K_2HPO_4, ≥99.0%), ammonium chloride (NH_4Cl, ≥99.0%)potassium chloride (KCl, ≥99.0%), sodium chloride (NaCl, ≥99.0%), magnesium chloride ($MgCl_2$, ≥98.0%), potassium ferrocyanide ($K_3[Fe(CN)_6]$, ≥98.5%), potassium ferricyanide ($K_4[Fe(CN)_6]$, ≥99.0%), tetrahydrafuran (THF, anhydrous ≥99.0%), dichloromethane (DCM, anhydrous ≥99.0%), methanol (anhydrous ≥99.0%), Methacrylic acid (MAA, 99%), ethylene glycol methacrylate (EDMA, 98.0%), 2,2`-azobis (2-methylpropionitrile) (AIBN, recrystallized 99.0%), acetic acid (≥99.0%), hydrocortisone (HPLC grade, ≥98.0%), progesterone (≥99.0%), cortisone (≥98.0%), testosterone (≥98.0%), high molecular weight polyvinyl chloride (PVC, M_w ~80kDa and M_n ~47kDa), bis(2-ethylhexyl) adipate (≥98.0%), potassium tetrakis(4-chloropheny1)borate (KT_4ClPB, ≥98.0%), ethyleneglycol (EG, ≥XX%), dodecylbenzenesulfonic acid (DBSA, ≥95%), and (3-Glycidyloxypropyl)trimethoxysilane (GOPTS, ≥98%) were purchased from Sigma-Aldrich (St. Louis, MO, USA) and were used without further purification. Aqueous solutions were prepared with Milli-Q water (18.2 MΩ·cm) obtained by Millipore system (Billerica, MA, USA). The medical grade adhesive tapes were obtained by generous donation of 3M© (USA). The double sided (1521) and single-sided (1509) medical tapes on a roll consist of a 3-millimeter transparent polyethylene film, coated on two sides for double-sided and single side for single-sided tape with a non-tackifier acrylic adhesive.

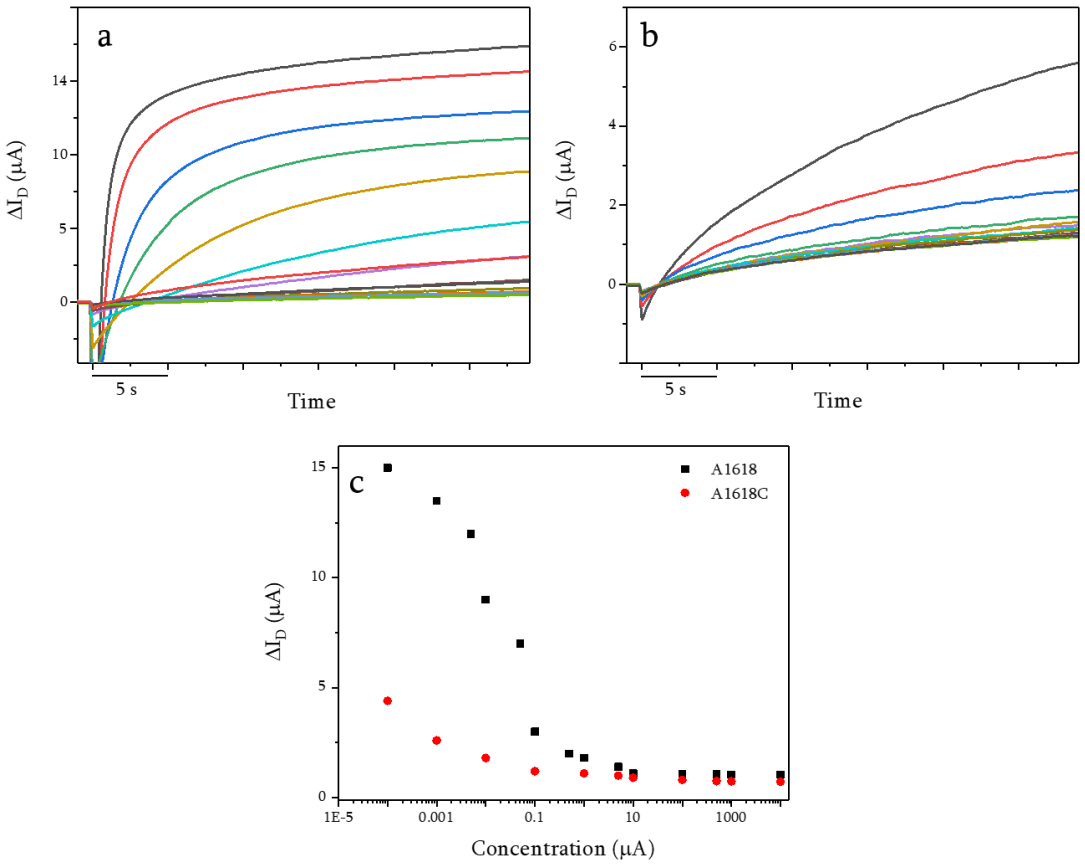

Fig. S1. Ex situ device testing for A1618 and A1618C. *Ex-situ* drain-current measurement for molecularly-imprinted (A1618) (**A**) and non-imprinted (A1618C) (**B**) polymers-based membranes, and their corresponding calibration curves (**C**).

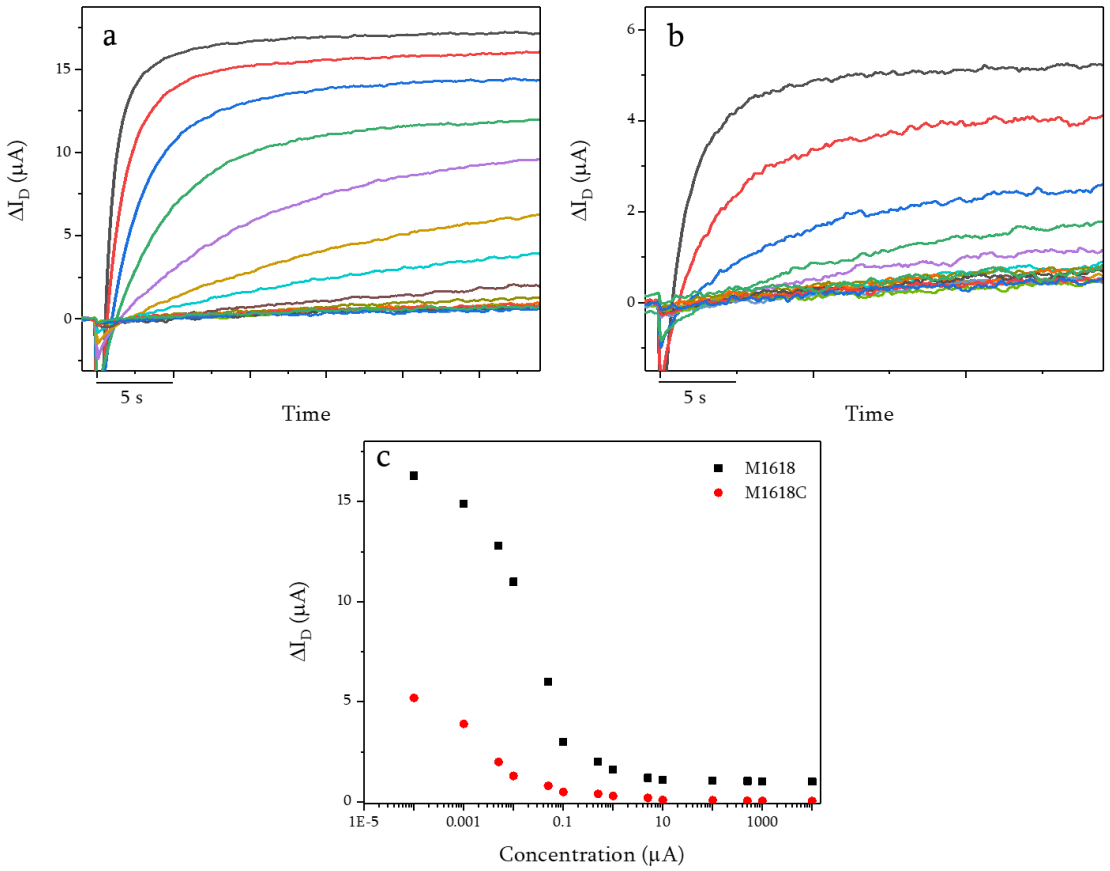

Fig. S2. Ex situ device testing for M1618 and M1618C. *Ex-situ* drain-current measurement for molecularly-imprinted (M1618) (**A**) and non-imprinted (M1618C) (**B**) polymers-based membranes, and their corresponding calibration curves (**C**).

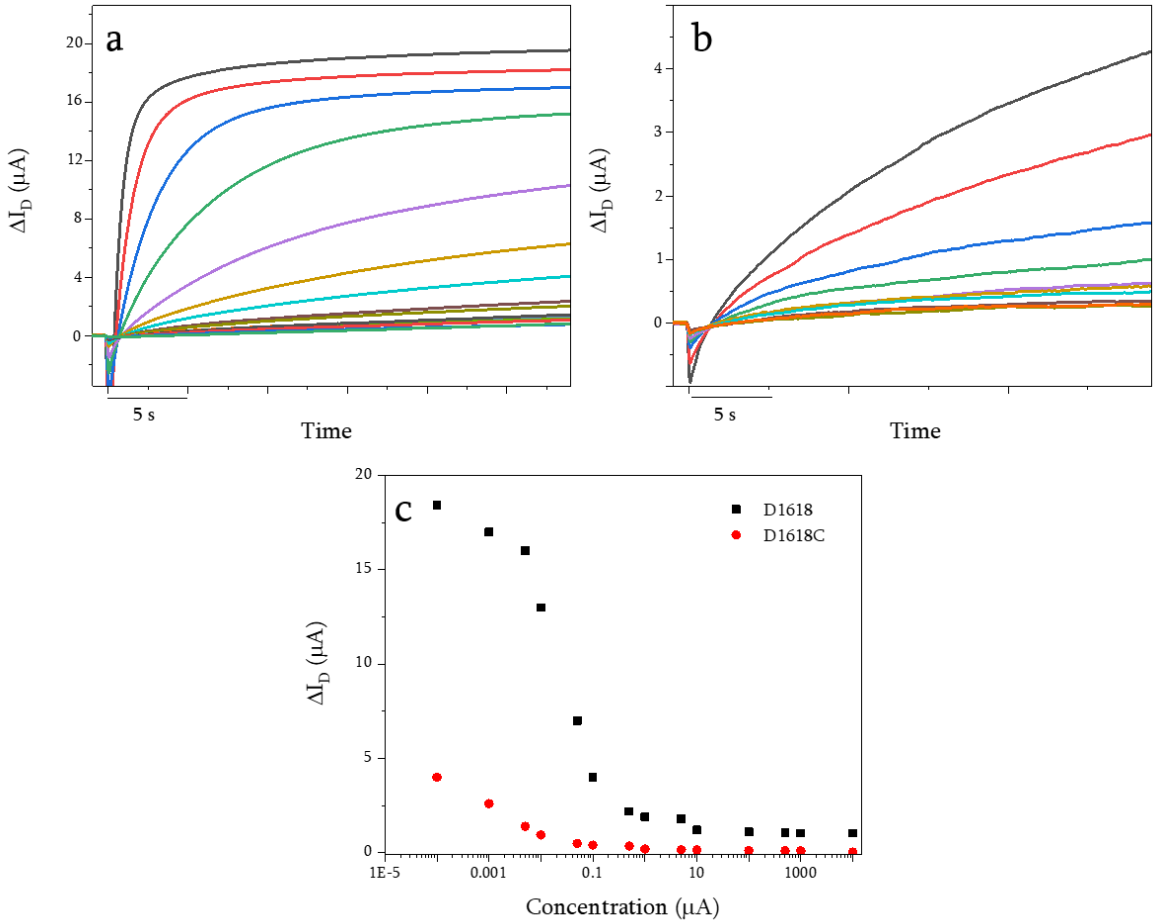

Fig. S3. Ex situ device testing for D1618 and D1618C. *Ex-situ* drain-current measurement for molecularly-imprinted (D1618) (**A**) and non-imprinted (D1618C) (**B**) polymers-based membranes, and their corresponding calibration curves (**C**).

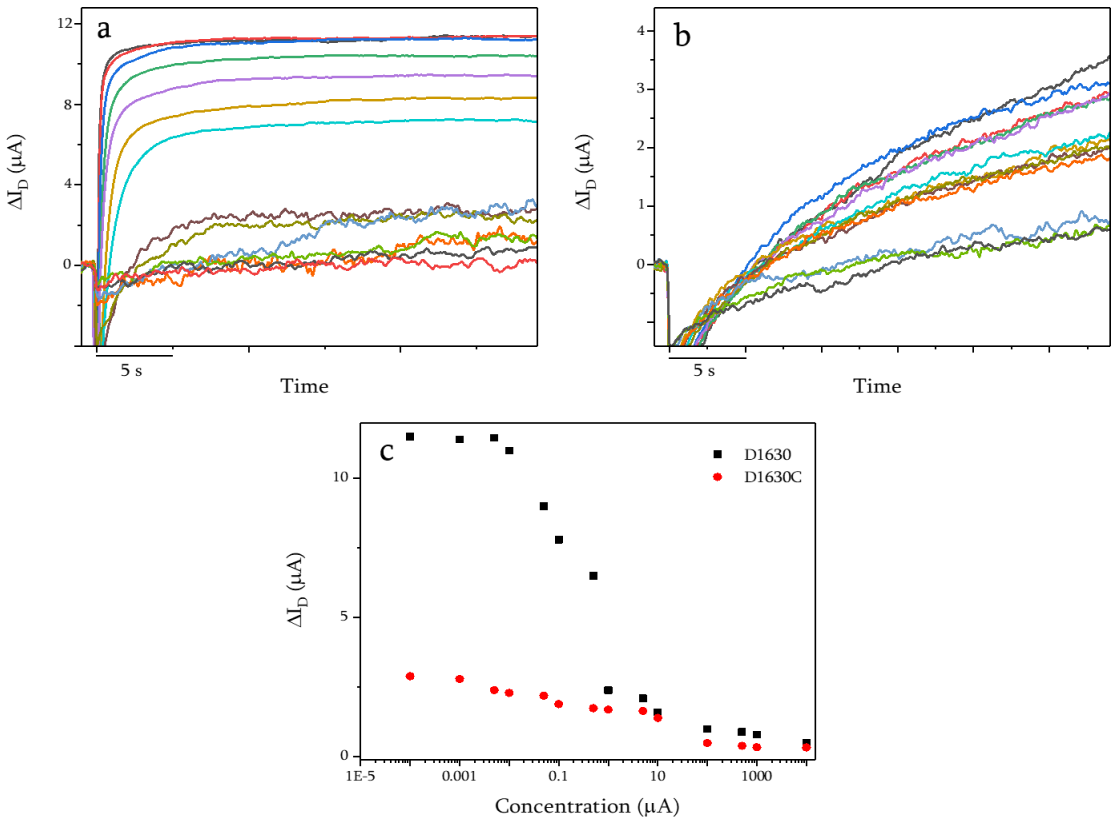

Fig. S4. Ex situ device testing for D1630 and D1630C. *Ex-situ* drain-current measurement for molecularly-imprinted (D1630) (**A**) and non-imprinted (D1630C) (**B**) polymers-based membranes, and their corresponding calibration curves (**C**).

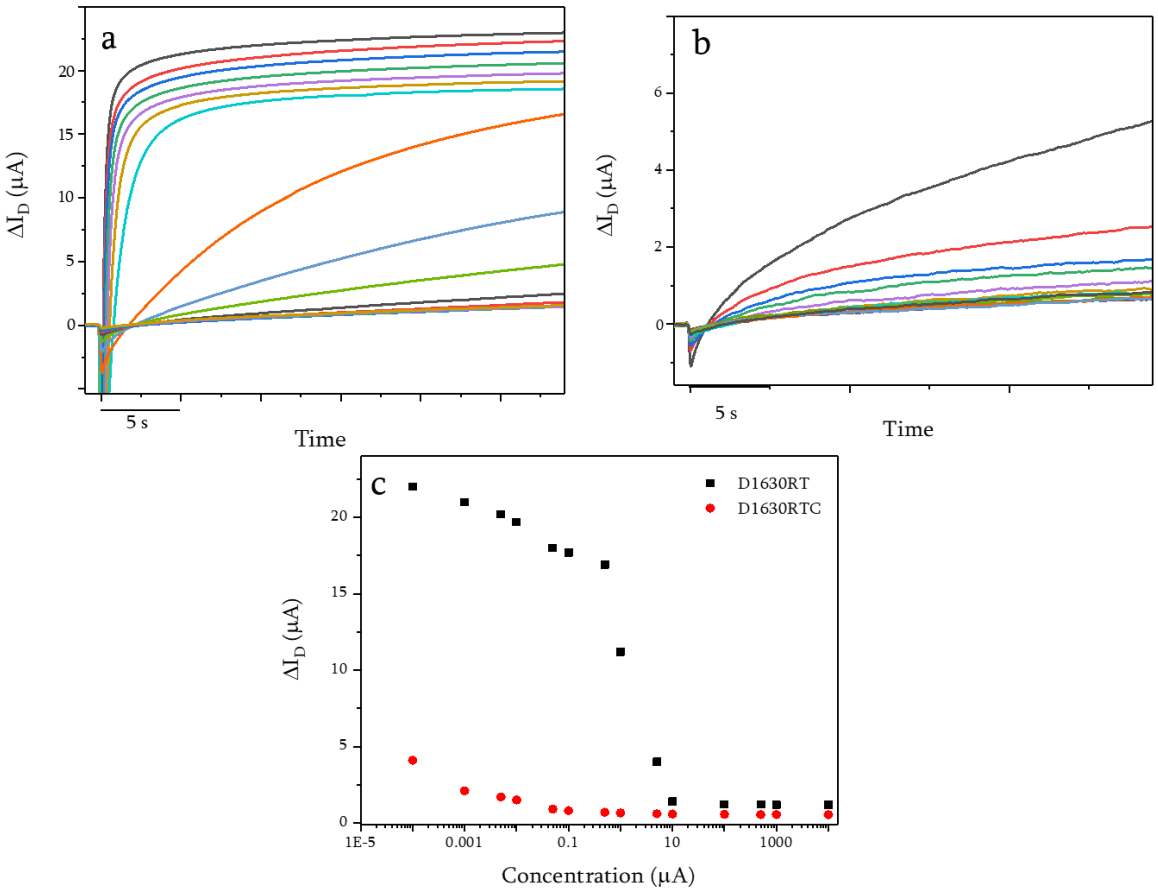

Fig. S5. Ex situ device testing for D1630RT and D1630RTC. *Ex-situ* drain-current measurement for molecularly-imprinted (D1630RT) (**A**) and non-imprinted (D1630RTC) (**B**) polymers-based membranes, and their corresponding calibration curves (**C**).

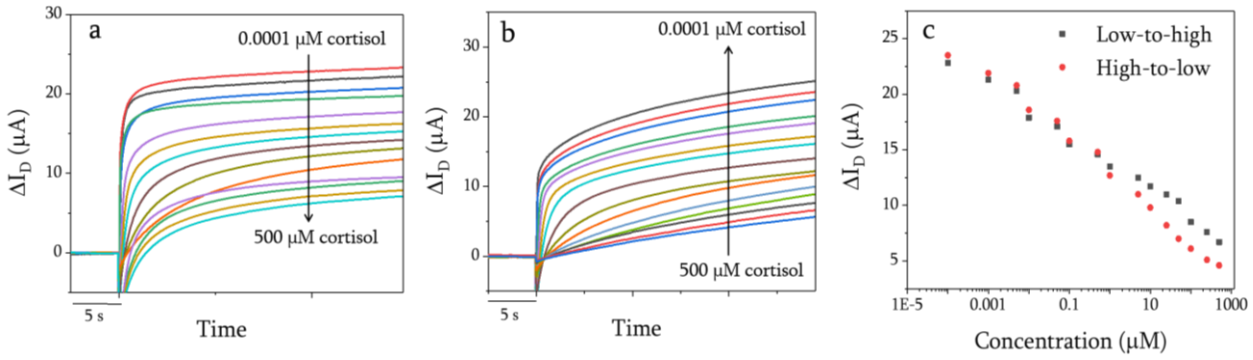

Fig. S6. Reversibility test for unsaturated device. *Ex-situ* drain-current measurements for molecularly-selective membrane-based sensor device (MSM) by gradually increasing (low-to-high) (**A**) and decreasing (high-to-low) (**B**) cortisol concentrations in artificial sweat and their corresponding calibration curves (**C**). The concentration range is kept 0.0001 μM to 500 μM in unsaturated regime.

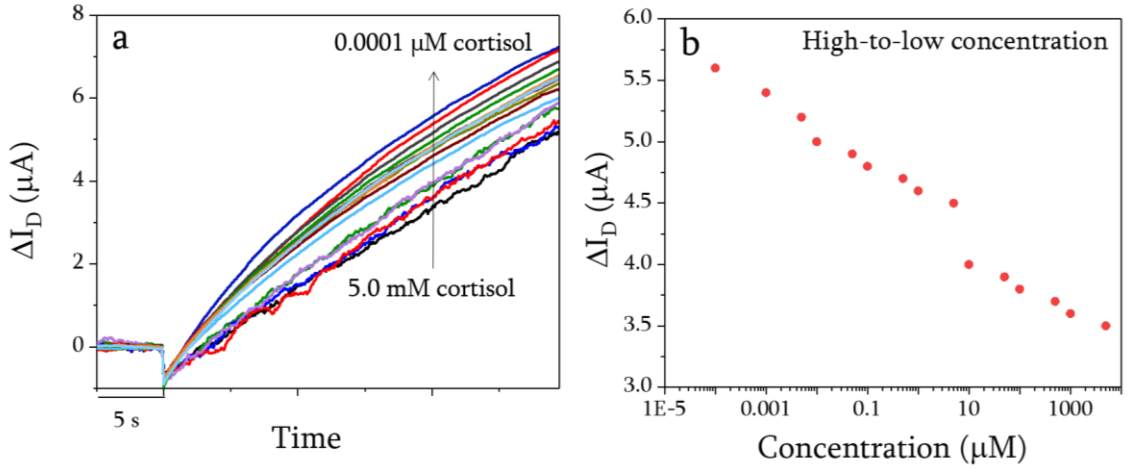

Fig. S7. Reversibility test for saturated device. *Ex-situ* drain-current measurements for molecularly-selective membrane-based sensor device (MSM) by decreasing (high-to-low) cortisol concentrations in artificial sweat (b) and its corresponding calibration curve (b). The concentration range is kept 0.0001 μM to 5.0 mM in saturated regime.

Table S1. BET characteristics. The specific surface area of polymer formulations and their control was evaluated by nitrogen physiosorption using a Brunauer-Emmett-Teller (BET) Quantachrome Autosorb iQ3 instrument. The samples were degassed under vacuum at 80°C for 6 hours prior to analysis. The pore size was determined using the desorption isotherms in a relative pressure window from 0.35 to 0.99, and following the Barrett-Joyner-Halenda (BJH) approach.

Membrane	Surface Area (m^2/g)	Pore Volume (cm^3/g)	[a]Pore Diameter (nm)
A1618	36.8	0.44	3.0
A1618C	21.1	0.21	3.1
M1618	66.4	0.65	3.7
M1618C	26.5	0.21	3.7
D1618	44.8	0.48	4.2
D1618C	13.8	0.11	3.3
D1630	231.8	2.7	3.7
D1630C	28.1	0.28	3.9
D161860	26.6	0.21	3.7
D161860C	13.8	0.12	3.7
D161860RT	101.1	0.84	3.5
D161860RTC	65.7	0.39	3.7

[a]BJH method was applied to calculate pore size distribution from experimental isotherms using the Kelvin model of pore filling. The method applies only to the mesopore and small macropore size range.

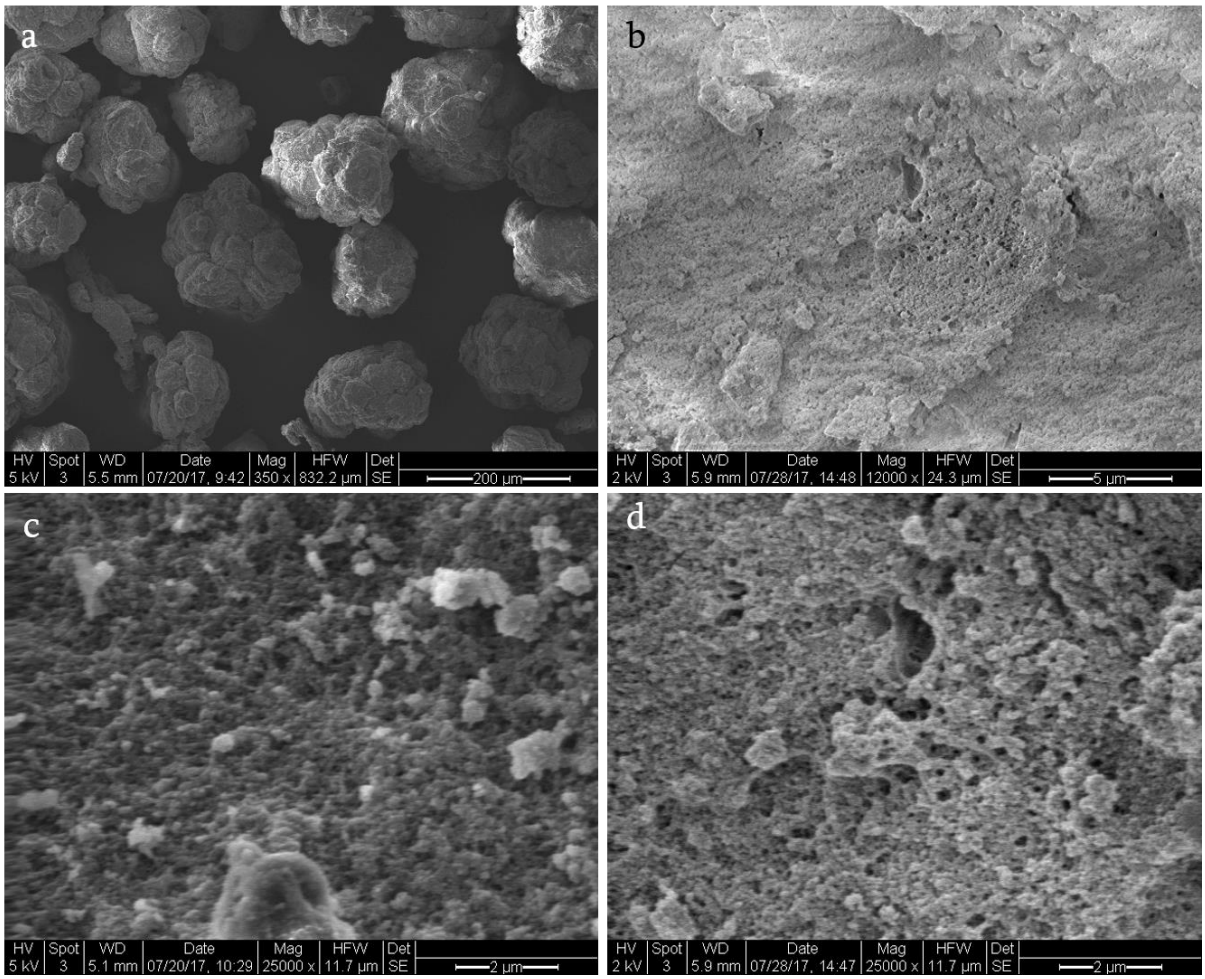

Fig. S8. SEM characterization of MIP. Scanning Electron Microscopy images for molecularly-imprinted polymer (D1630) with increasing magnification (**A** to **D**).

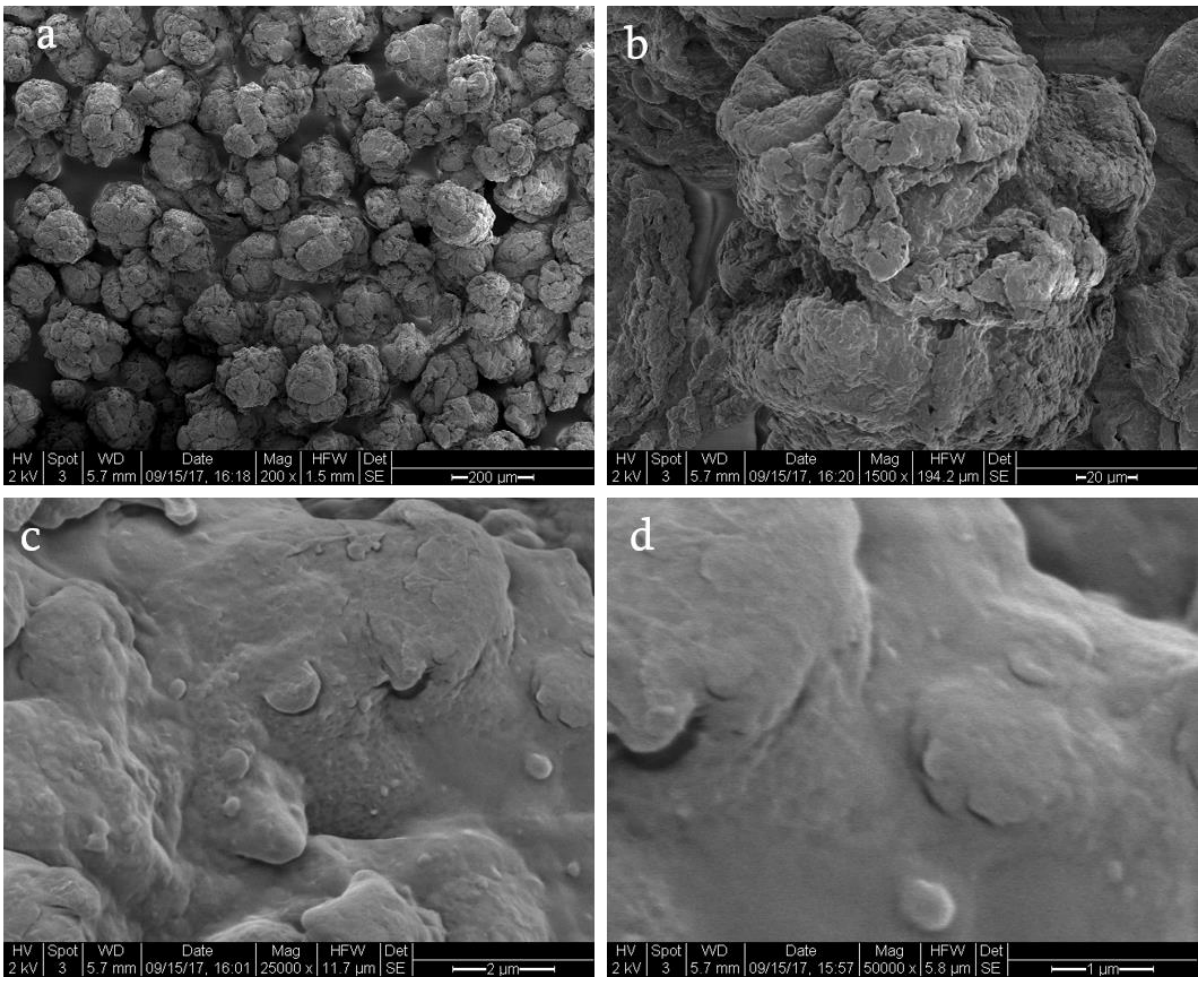

Fig. S9. SEM characterization of NIP. Scanning Electron Microscopy images for non-imprinted polymer (D1630C) with increasing magnification (**A** to **D**).

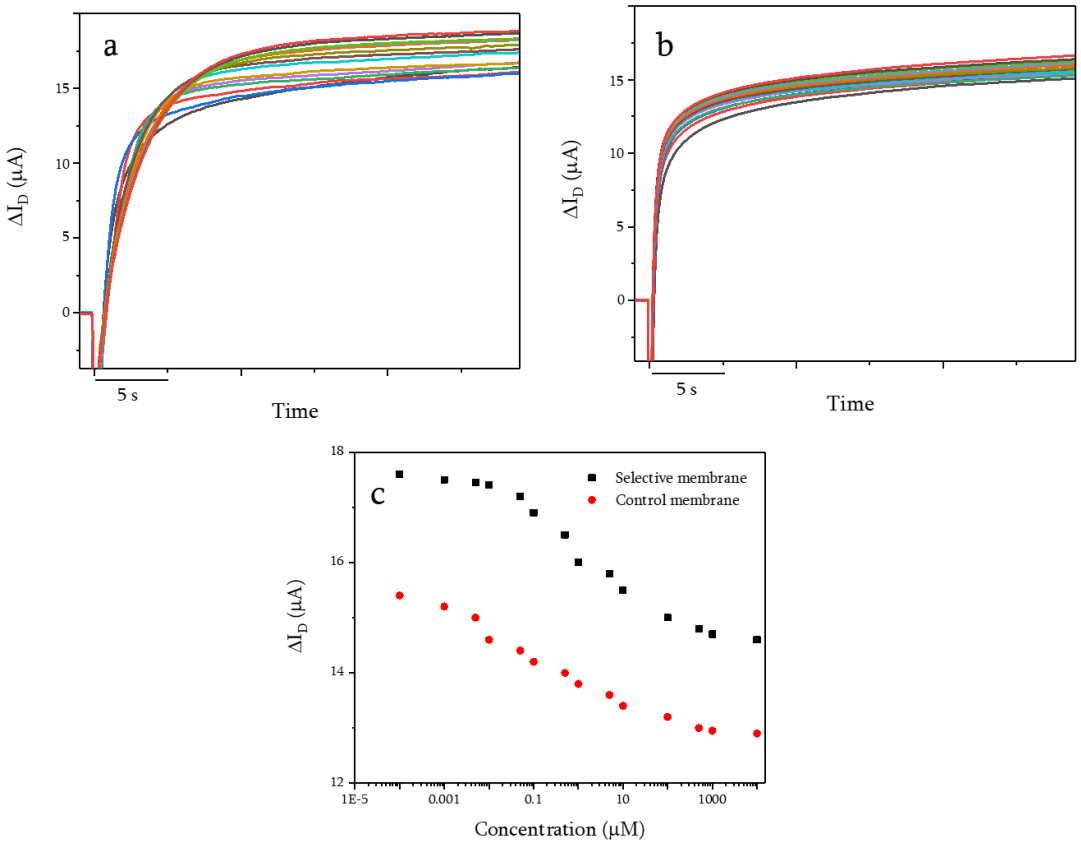

Fig. S10. Drain current measurements without PVC matrix. *Ex-situ* drain-current measurement with increasing concentrations of cortisol in artificial sweat for molecularly-imprinted (**A**) and non-imprinted (**B**) polymers without any PVC host matrix, and their corresponding calibration curves (**C**).

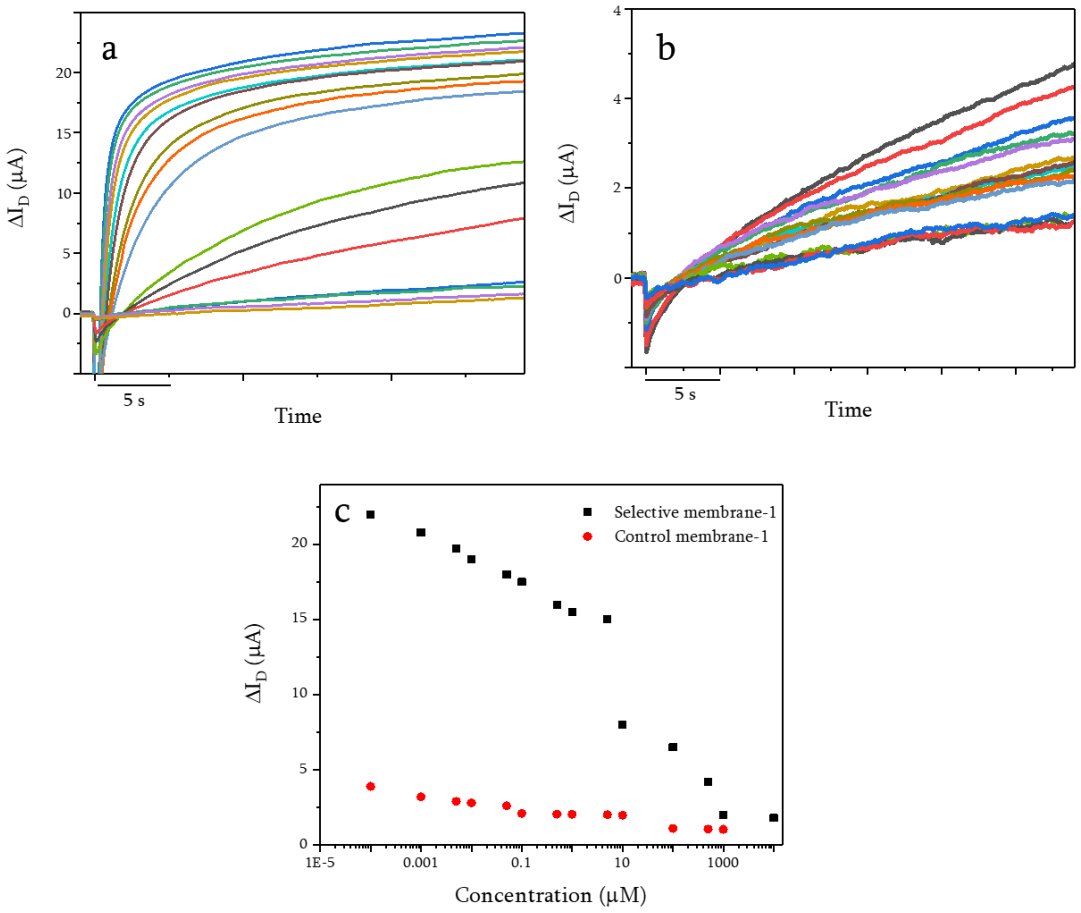

Fig. S11. Drain current measurements in 10% PVC matrix. *Ex-situ* drain-current measurement with increasing concentrations of cortisol in artificial sweat for molecularly-imprinted (**A**) and non-imprinted (**B**) polymers with 10% in PVC host matrix, and their corresponding calibration curves (**C**).

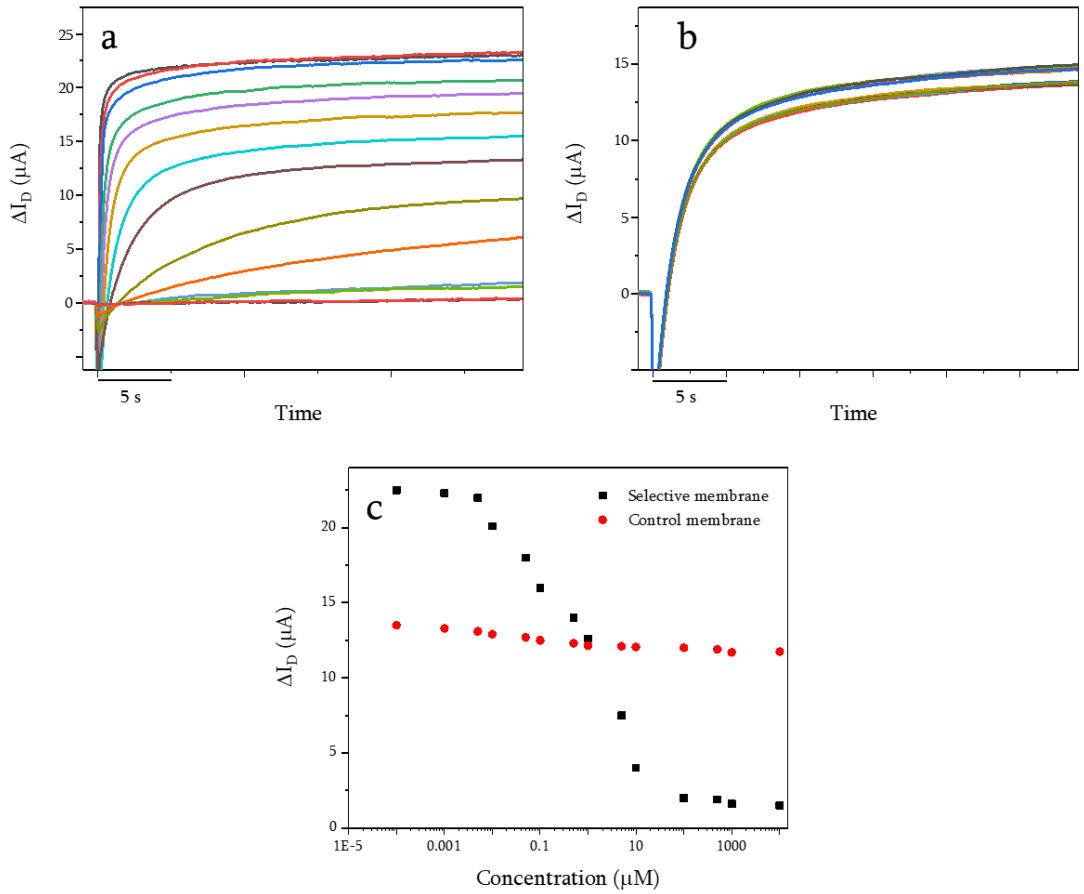

Fig. S12. Drain current measurements in 25% PVC matrix. *Ex-situ* drain-current measurement with increasing concentrations of cortisol in artificial sweat for molecularly-imprinted (**A**) and non-imprinted (**B**) polymers with 25% in PVC host matrix, and their corresponding calibration curves (**C**).

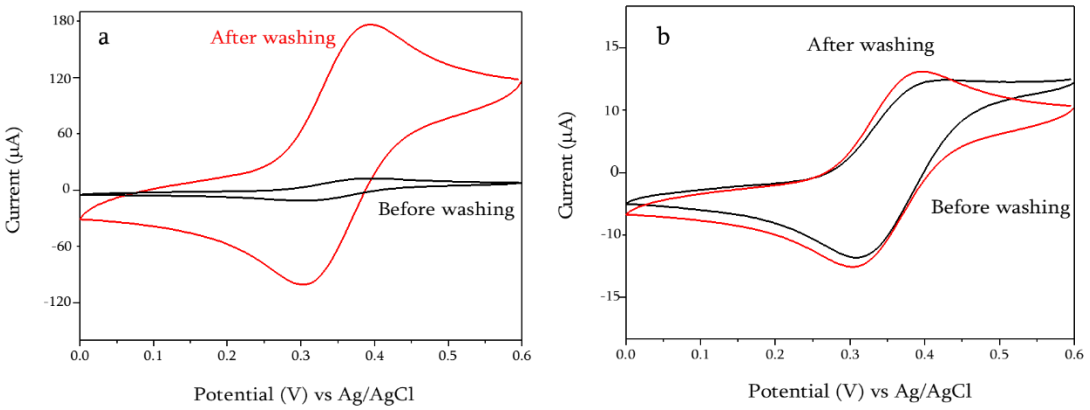

Fig. S13. Washing tests by cyclic voltammetry. Cyclic voltammogram of molecularly-selective polymer (D1630) integrated OECT before (black curve) and after (red curve) washing treatment to remove cortisol from final membrane (**A**), and cyclic voltammogram for non-imprinted polymer (D1630C) before (black curve) and after (red curve) (**B**) washing treatment. Washing process was applied using acetic acid:methanol mixture (8:2 v/v). Washing solution was applied to membranes by first dispersing particles in centrifuge tube, and shake for 30 minutes, then centrifuged at 1000 rpm for 15 minutes. This process was applied 5 times, successively to each membrane.

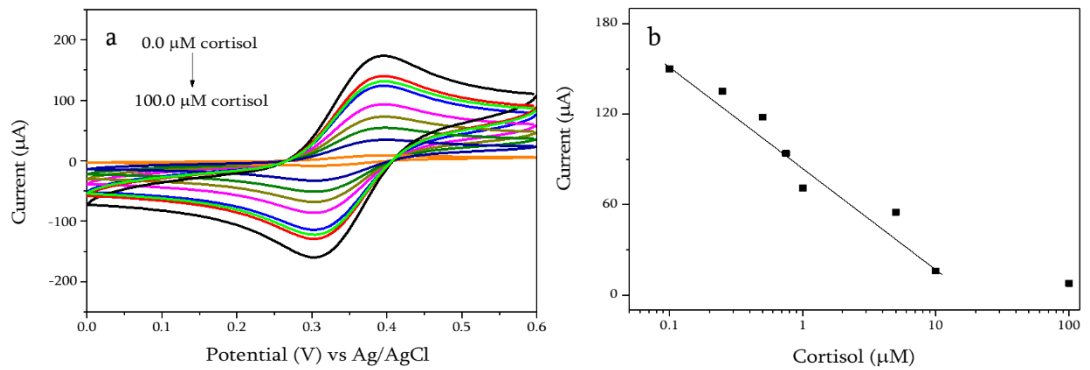

Fig. S14. Diffusion characteristics of the MS-OECT. Cyclic voltammogram of MS-OECT device in artificial sweat containing 5 mM $[Fe(CN)_6)]^{3-/4-}$ with increasing concentration of cortisol (**A**) and corresponding peak current *vs* cortisol concentration (**B**).

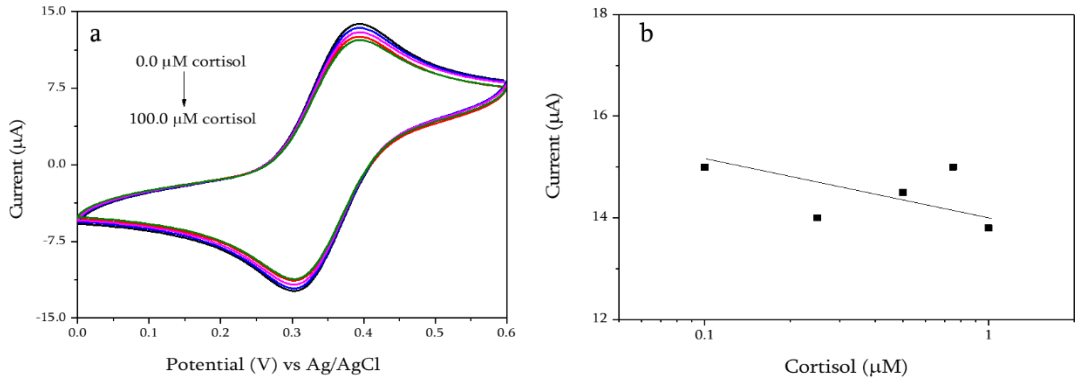

Fig. S15. Diffusion characteristics of the NS-OECT. Cyclic voltammogram of MSC-OECT device in artificial sweat containing 5 mM $[Fe(CN)_6)]^{3-/4-}$ with increasing concentration of cortisol (**A**) and the corresponding peak current *vs* cortisol concentration (**B**).

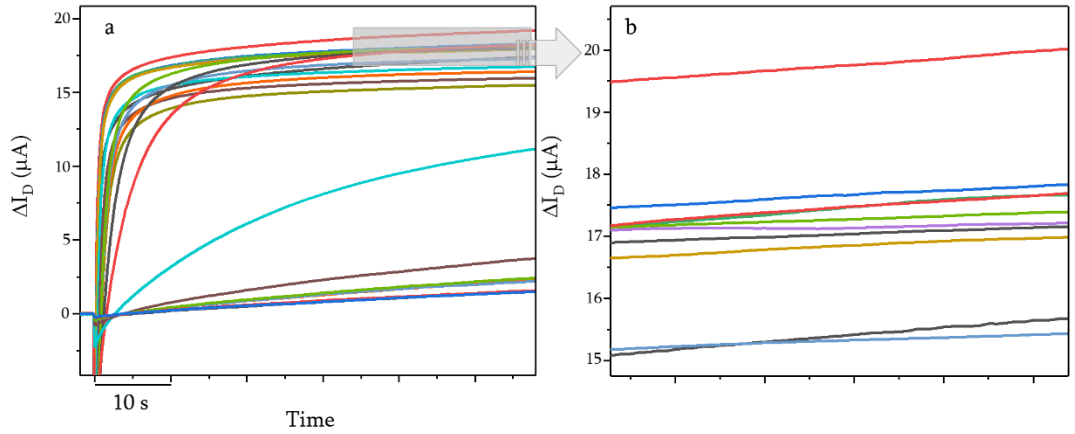

Fig. S16. Selectivity tests. Drain-current measurement for MS-OECT for selectivity test (**A**), highlighted area (**B**). The measurements were conducted in artificial sweat with increasing concentrations of cortisol. The selectivity of the MS-OECT device was evaluated in the presence of structural analogs of cortisol including progesterone, cortisone and testosterone in artificial sweat. The measurement was started with 0.005 mM cortisol and it was gradually increased up to 5.0 µM. The concentrations of interferent were increased step-wise for progesterone, to ensure that they do not involve binding process.

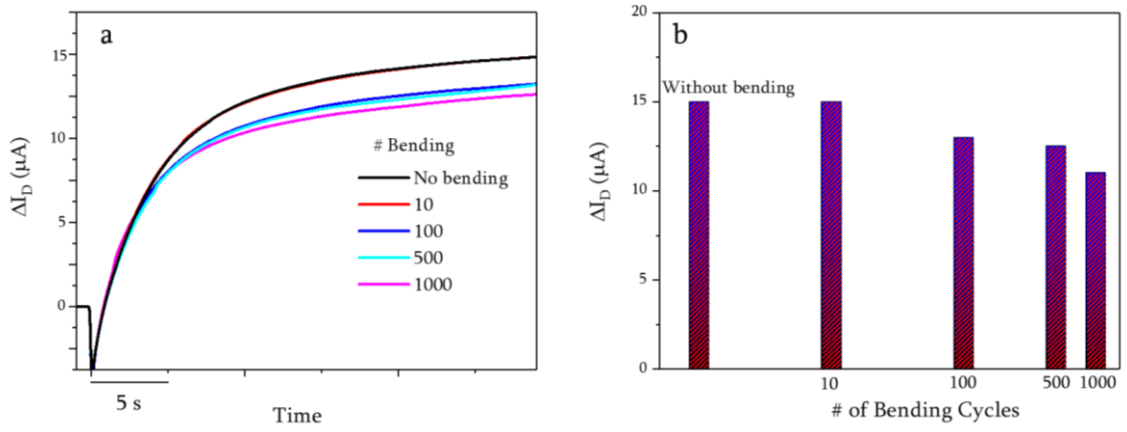

Fig. S17. Bending tests. Bending test for MS-OECT with increasing bending cycles represented by drain-current measurement (**A**) and histogram for corresponding peak currents (**B**). The ex-situ measurements were conducted in artificial sweat with constant concentration of cortisol.

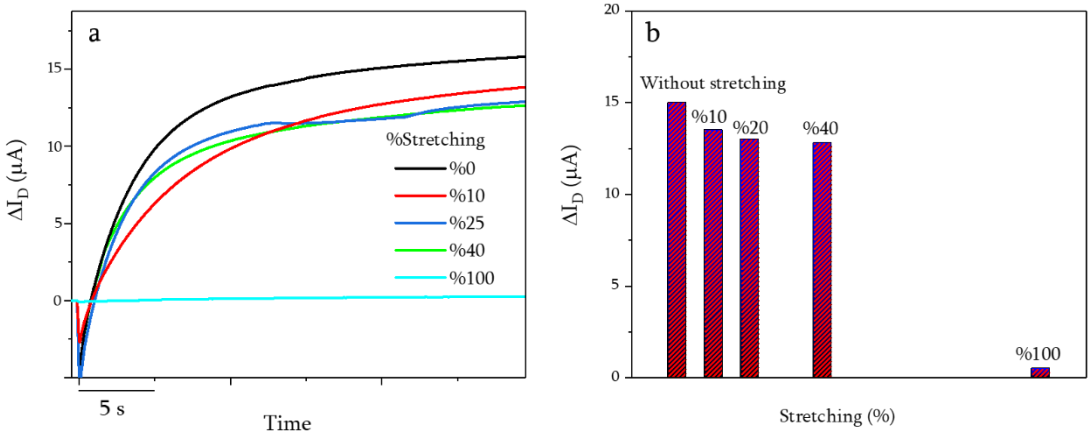

Fig. S18. Stretchability tests. Stretching test for MS-OECT with different strain represented by drain-current measurement (**A**) and histogram for corresponding peak currents (**B**). The ex-situ measurements were conducted in artificial sweat with constant concentration of cortisol.

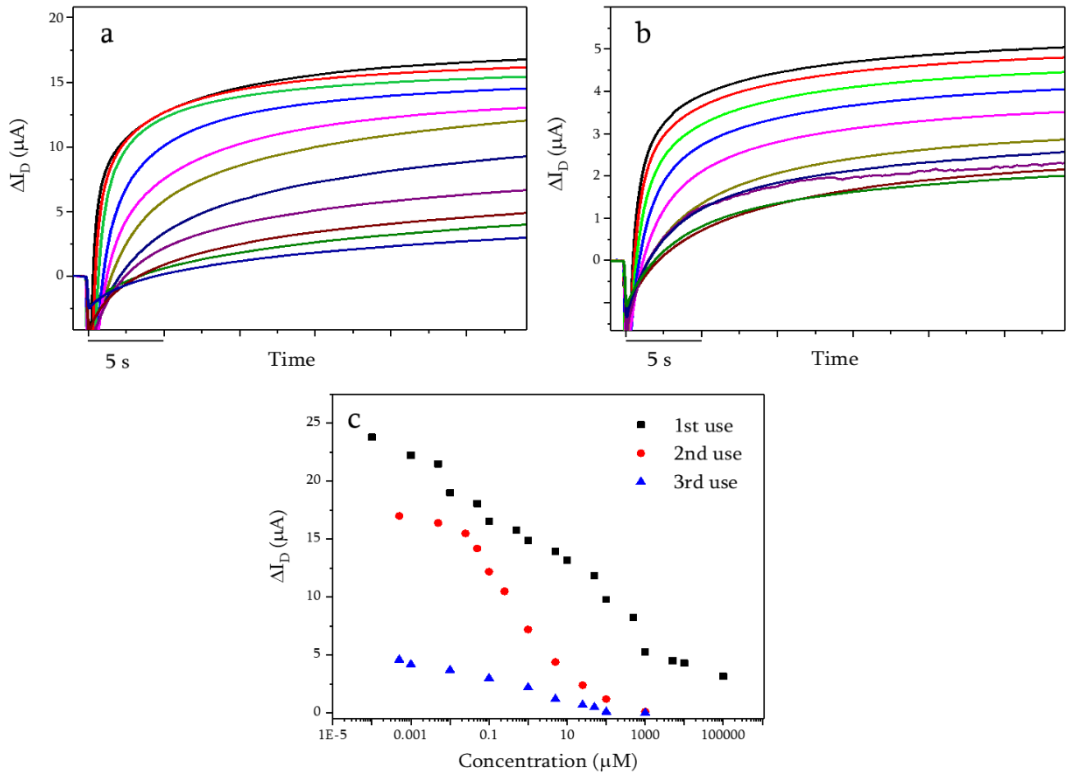

Fig. S19. The reusability tests. *Ex-situ* drain-current measurement of MS-OECT device for reusability test in artificial sweat with increasing concentration of cortisol. Output currents for second (**A**) and third (**B**) use of device without applying extra washing process. Calibration curve for panel a and b (**C**).

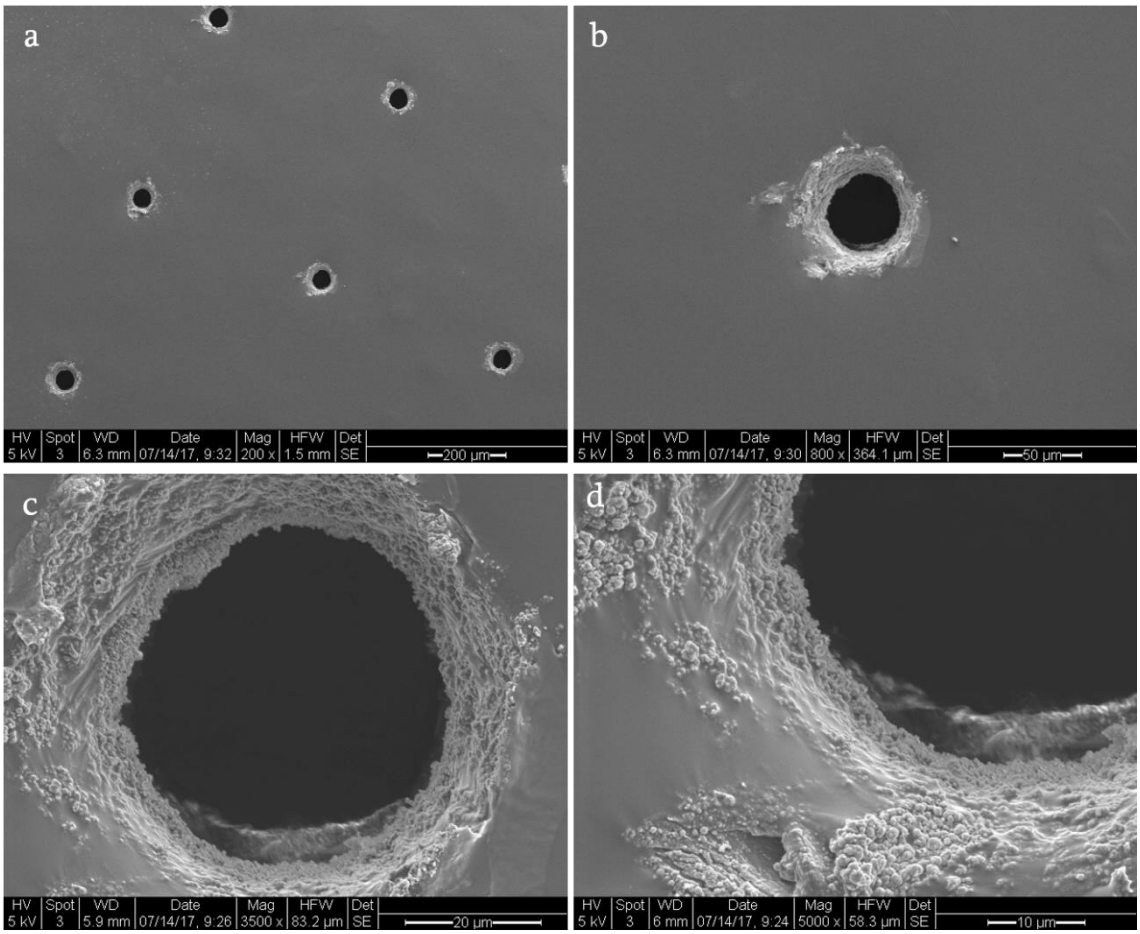

Fig. S20. SEM characterization of microchannel arrays. Scanning Electron Microscopy (SEM) images for laser-pattern microcapillary channels with increasing magnification (**A** to **D**).

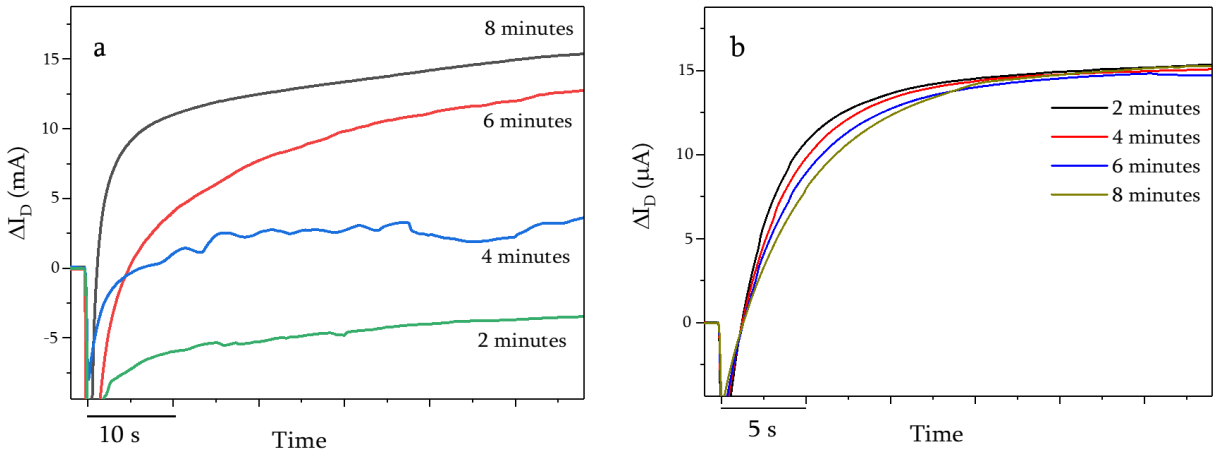

Fig. S21. The performance of acquisition layer. Drain-current comparison for devices with a punch-hole (**A**) and laser-patterned (**B**) sampling layer. Tests were performed using same solution (artificial sweat) with same volume (100 μL) and applied to same forearm and measured at 2-minute intervals.

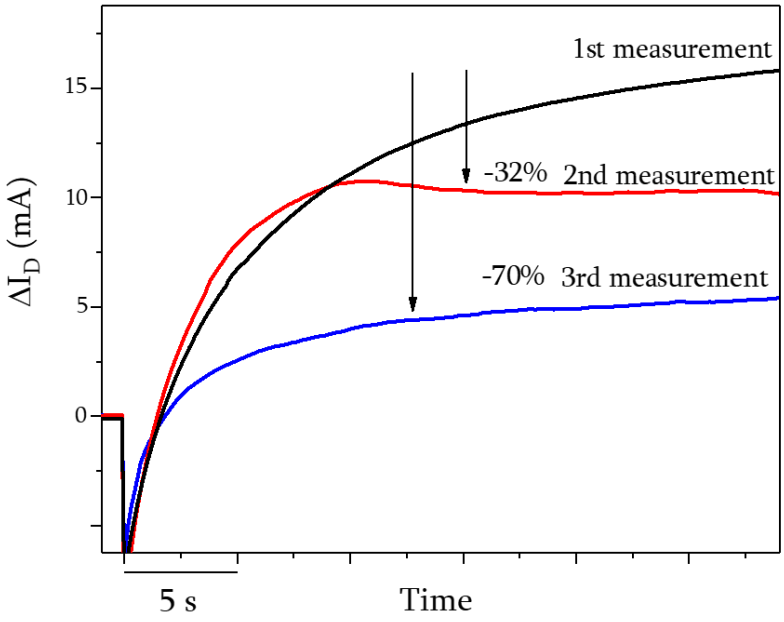

Fig. S22. The reusability test for on-body real sample analysis. The results show that device performance was decreased 32% (red curve) and 70% (blue curve) for second and third use, respectively. 2nd and 3rd measurements were conducted without washing/sonicating the device.

Note S1. Nanopore formation in MIP.

The MIP polymerization usually starts with the decomposition of the radical initiator, and polymer chains start to grow and progressively form a gel that precipitates because of high-crosslinking. The polymerization continues and the growing nuclei collapse to form globules. At the end of polymerization, globules and clusters form the units of microporous polymer. The difference of shapes and structure of selective and control polymer are from the different interactions between template-monomer and template-solvent molecules. The presence of template causes a delay in the precipitation and nucleation processes, leading to better solubility of the polymer and as a result formation of smaller pores. In the case of the NIP, it may be the case that precipitation occurs earlier and progresses quicker, causing larger pore formation.

Note S2. Rationale for MIP design.

The first cortisol-selective MIP was prepared using methacrylic acid (MAA) and ethylene glycol dimethacrylate (EDMA) as monomer and cross-linker, respectively. MAA monomer was used due to its carboxylic acid group which establishes hydrogen bonds as a donor, giving rise to electrostatic bonds with solvent molecules. Another reason for choosing MAA is that it does not react with cortisol during polymerization. EDMA is used as a cross-linker because it helps to increase hydrophilicity of final polymer and it is a bifunctional cross-linker that makes the polymer more flexible compared to its trifunctional counterparts. To test the effect of the solvent, we used three solvents including acetonitrile, methanol and dichloromethane (DCM) under the same template/monomer/cross-linker ratio and polymerization conditions (A1618, M1618, D1618, respectively). The Brunauer-Emmett-Teller (BET) surface area and porosity measurements show that using DCM as a solvent leads the higher surface area, bigger pore diameter and pore volume (table S1, Supporting Information). After choosing the best solvent, different template/monomer/cross-linker ratios were tested in DCM. We used three different ratios by increasing cross-linker concentration by three and five-folds with respect to template/monomer concentration (D1630, and D1660). The results show that. Cross-linker concentration also plays an important role in the final physicochemical properties of the MIP, particularly its hydrophilicity/hydrophobicity. The results demonstrate that the MIP prepared by five-folds cross-linker concentration (D1660) yields a rigid and poorly soluble polymer, and as a result showed the lowest sensing factor among all trials. Finally, with the best monomer/cross-linker ratio and solvent, polymerization conditions were varied (D1630 and D1630RT). We compare two different reaction temperatures for 4 ℃ for D1630, and room temperature for D1630RT while keeping other polymerization conditions constant. The results show that lower temperature favored the complex formation because the electrostatic and hydrogen bonding interactions are more stable at lower temperature.

Note S3. Diffusion characteristics of MSM.

The diffusion characteristics of all transistor devices before and after integrating with MSM and a control non-selective membrane (NSM) were characterized by measuring voltammetric responses in solution containing 5mM $[Fe(CN)_6)]^{3-/4-}$ in artificial sweat with various concentrations of cortisol. Figure S14-15 shows the voltammetric responses of each transistor device with MSM (fig. S14a) and NSM (fig. S15a) in constant electrolyte concentrations with an increasing concentration of cortisol. Both of the devices displayed a classical sigmoidal shape with different peak-to-peak potential separations and showed narrow peak-to-peak separations, indicating fast electron transfer. The effect of scan rates on the cathodic (I_{pc}) and anodic peaks (I_{pa}) of both devices were shown in the Figure fig. S14b and fig. S15b for MEM-4, and Control-4, respectively. Both anodic and cathodic peak currents increased linearly with increasing scan rates (10 to 300mVs^{-1}) for MSM, which suggest a typical diffusion-controlled electrode process. However, peak currents remain almost same for the control membrane because there is no cortisol-binding.